Running Head: Killer whale condition and survivorship

Full Title: Survival of the Fattest: Linking body condition to prey availability and survivorship of killer whales

Joshua D. Stewart[1*], John W. Durban[2,3], Holly Fearnbach[4], Lance G. Barrett-Lennard[5], Paige K. Casler[6], Eric J. Ward[7], Derek R. Dapp[8]

Affiliations

[1]*National Research Council Postdoctoral Fellow for Marine Mammal and Turtle Division, Southwest Fisheries Science Center, National Marine Fisheries Service, National Oceanic and Atmospheric Administration, La Jolla, CA*
[2]*Marine Mammal and Turtle Division, Southwest Fisheries Science Center, National Marine Fisheries Service, National Oceanic and Atmospheric Administration, La Jolla, CA*
[3]*Southall Environmental Associates, Inc., Aptos, CA*
[4]*SR3, SeaLife Response, Rehabilitation and Research, Des Moines, WA*
[5]*Ocean Wise Conservation Association, Vancouver, BC*
[6]*Ocean Associates, Inc., in support of Marine Mammal and Turtle Division, Southwest Fisheries Science Center, National Marine Fisheries Service, National Oceanic and Atmospheric Administration, La Jolla, CA*
[7]*Conservation Biology Division, Northwest Fisheries Science Center, National Marine Fisheries Service, National Oceanic and Atmospheric Administration, Seattle WA*
[8]*Washington Department of Fish and Wildlife, Olympia, WA*

*Corresponding Author: joshua.stewart@noaa.gov

Abstract

Recovering small, endangered populations is challenging, especially if the drivers of declines are not well understood. While infrequent births and deaths may be important to the outlook of endangered populations, small sample sizes confound studies seeking the mechanisms underlying demographic fluctuations. Individual metrics of health, such as nutritive condition, can provide a rich data source on population status and may translate into population trends. We use aerial photogrammetry data to build a Bayesian predictive model of body condition changes in endangered Southern Resident killer whales (SRKWs), providing a unique test case comprising decades of demographic monitoring, a small population size, and repeated condition measurements of individual whales. We demonstrate that fluctuations in SRKW body condition can be explained by the abundance of Chinook salmon, providing targeted management opportunities. We also show that whales in poor body condition—reflecting depleted fat reserves—are more likely to die, linking changes in condition to population viability.

Key words: *Orcinus orca*; resident killer whale; foraging ecology; body condition; drones; photogrammetry; adaptive management; multi-state modeling.

Introduction

Endangered species with small population sizes approaching extinction or local extirpation present a diversity of management challenges (Soulé 1987, Dennis 1989). When the causes of population declines are not well established it is difficult to identify management strategies that will prevent declines and promote recovery. Studies of small populations by definition suffer from sample size limitations (Walsh 2000, Brosi and Biber 2009), complicating efforts to identify stressors that may be influencing population trends (Schönbrodt and Perugini 2013). For example, infrequent births or deaths may have dramatic impacts on population trends, but may be too sparse to identify mechanisms. In these cases, non-invasive metrics of individual health can help identify drivers of population trends and allow for management strategies that preempt demographic casualties that impact population viability, such as the loss of reproductive females.

Nutritive condition in long-lived vertebrates can provide a sensitive signal of short-term individual or population health. Changes in condition may reflect changes in the environment or foraging success, and persistent variation may translate into population trends (Berger 2012, Boulanger et al. 2013, Vindenes et al. 2014). Aerial imaging technology has provided one example of such non-invasive individual health metrics (Perryman and Lynn 2002). Photogrammetry with remotely controlled drones has been used increasingly over the past 5-10 years as drones have become cheaper, safer and more efficient compared with traditional photogrammetry using manned aircraft (Durban et al. 2015). These methods have been widely applied to both terrestrial and marine species (Perryman et al. 2014, Hu et al. 2020). Working with marine or other aquatic organisms is particularly challenging, as individuals are highly mobile and may spend little time near the surface where they can be imaged. Nevertheless, aerial

photogrammetry has been used to collect individual measurements of marine mammal species including investigations of life history characteristics (Christiansen et al. 2016, Groskreutz et al. 2019) and nutritive condition (Christiansen et al. 2018, Fearnbach et al. 2018, 2019). A strength of aerial photogrammetry is that it can non-invasively provide quantitative metrics of body condition at the individual level (Durban et al. 2015, Fearnbach et al. 2018), which can be used to evaluate the health or status of a large portion of a population in near real time. Demographic trend data, in contrast, has high inherent variability in small populations and may need to be collected for years before it provides reliable inferences about population health.

Collecting individual health data from wild populations may be challenging, particularly if individuals can't be identified or the population is not censused. Killer whales (*Orcinus orca*) represent an ideal case for relating individual health metrics to the environment, as population sizes are typically small, and individuals are readily identifiable. One of the smallest populations of killer whales, the Southern Resident killer whale (SRKW) population, is censused annually and demographic characteristics (age, sex) have been recorded for the entire population since the mid 1970s (Center for Whale Research 2020). This small (n=73) population of fish-eating killer whales is found in the eastern north Pacific (Ford et al. 1998) with a range including coastal waters from central California to Southeastern Alaska, and core summer habitat in the Salish Sea between Puget Sound and Southern Vancouver Island (National Marine Fisheries Service 2019). Because of its small size and a decline in abundance of approximately 25% since 1995, the SRKW population is listed as endangered under the Endangered Species Act (ESA) in the United States and the Species-at-Risk Act (SARA) in Canada. The diet of SRKWs comprises primarily Chinook salmon (*Oncorhynchus tshawytscha*), although other species such as coho salmon

117 (*Oncorhynchus kisutch*), chum salmon (*Oncorhynchus keta*), halibut (*Hippoglossus stenolepis*)
118 and groundfish have also been identified in their diets (Hanson et al. 2010, Ford et al. 2016).
119 Three main stressors are thought to be responsible for SRKW population declines: 1) elevated
120 levels of environmental pollutants in their core habitat range that could impact survivorship and
121 reproductive success (Krahn et al. 2009); 2) increasing vessel noise and disturbance in the Salish
122 Sea which could interfere with communication and foraging efficiency (Lusseau et al. 2009); and
123 3) declining Chinook salmon populations and therefore prey scarcity (Ford et al. 2010), which in
124 addition to direct effects could compound the other stressors.
125
126 Several studies have supported the hypothesis that prey limitation is a primary threat to the
127 SRKW population, linking aggregates of Chinook salmon abundance to both fecundity and
128 mortality (Ward et al. 2009, Ford et al. 2010, Vélez-Espino et al. 2014) as well as to declines in
129 adult body size (Fearnbach et al. 2011, Groskreutz et al. 2019). However, the range of both
130 SRKWs and their salmon prey is enormous, encompassing over 3,000km of coastline, and
131 identifying the prey populations that are most important for SRKWs is challenging. Chinook
132 salmon face a complex suite of stressors including habitat modification and degradation (Greene
133 and Beechie 2004), restricted access to spawning tributaries (Sheer and Steel 2006), fisheries
134 pressure (Ruckelshaus et al. 2002), increased natural mortality due to recovering marine mammal
135 populations (Chasco et al. 2017), and climate impacts (Crozier et al. 2008). Chinook populations
136 from four tributaries within the SRKW range are themselves listed as endangered in the United
137 States or Canada, with several others listed as threatened. To date, no studies have been able to
138 identify relationships between specific salmon populations and SRKW survivorship or
139 population health (Pacific Fishery Management Council 2020).

140

141 Aerial photogrammetry can provide a precise measure of individual killer whales' nutritive
142 condition by quantifying the relative amount of adipose fat stored behind the cranium; as
143 individuals decline in nutritive condition, they metabolize adipose fat in addition to blubber
144 stores (Fearnbach et al. 2019). As such, photogrammetry datasets potentially provide more
145 power to evaluate relationships between prey abundance and population status compared with
146 efforts to link prey to infrequent births and deaths. In this study, we used aerial photogrammetry
147 images of individually-recognizable SRKWs collected in 7 September field efforts across 12
148 years (2008-2019) to evaluate how changes in body condition might be related to the abundance
149 of different Chinook salmon populations. The SRKW population is composed of three distinct
150 collections of matrilineal family units (hereafter referred to as J, K and L pods) (Parsons et al.
151 2009) and we considered each pod separately in our analyses based on previously described
152 differences in range and movement patterns (Riera et al. 2019, National Marine Fisheries Service
153 2019).

154

155 **Methods**

156 *Data collection*

157 Aerial images of Southern Resident killer whales were collected in the Salish Sea near the San
158 Juan Islands, WA (Fearnbach et al. 2011, Groskreutz et al. 2019) in the month of September in
159 each of seven years. Images were collected from a manned helicopter in 2008 and 2013
160 (Fearnbach et al. 2011, 2018) and using a drone in 2015-2019 (Durban et al. 2015, Fearnbach et
161 al. 2019). Briefly, vertical images were collected using a digital camera at altitudes of 230-460 m
162 by helicopter and 25-45 m by drone. Despite changes in aircraft platforms, all images were

163 obtained with a Normal lens to ensure a flat image with no wide-angle distortion, with the
164 specific camera and lens chosen based on aircraft altitude to achieve a water-level pixel
165 resolution of 1-2cm (Durban et al. 2015). Research activities were permitted by the National
166 Marine Fisheries service in the U.S. and the Department of Fisheries and Oceans in Canada, and
167 aerial photogrammetry was approved as an observational (non-invasive) method by the
168 Institution Animal Care and Use Committee of the NOAA Southwest Fisheries Science Center
169 Marine Mammal and Turtle Division. Individual whales can be identified by unique markings
170 that are visible from aerial images, allowing measurements to be linked to individual whales of
171 known age and sex (Fearnbach et al. 2011, 2019, Durban et al. 2015). As a quantitative metric of
172 body condition we used the eye patch ratio (EPR), which is the ratio of the pixel distance
173 between the inside of the white eye patch pigmentation at their anterior end relative to their
174 distance at 75% of the eye patch length, described in Fearnbach et al. (2019) (Figure 1). The eye
175 patch ratio is a sensitive metric of nutritive condition as it measures the relative amount of
176 adipose fat stored behind the cranium. As killer whales become nutritionally stressed, they lose
177 this adipose tissue along with blubber fat reserves, resulting in lower EPRs, and as such this is a
178 more sensitive metric of nutritive condition in killer whales compared to other commonly used
179 metrics such as head width to body length ratios (Fearnbach et al. 2019). Multiple measurement-
180 quality images were available of a single whale on a given day and within years, and we used the
181 mean EPR for each whale in each year because EPR calculations had very low variability (e.g.
182 typical coefficients of variation of 0.003 to 0.008 for within year variability of a given whale)
183 (Fearnbach et al. 2019).
184
185 *Accounting for age & sex*

186 To prepare the raw eye patch ratio data for analysis, we first fit a generalized additive model to
187 the EPRs using the mgcv package (Wood 2006) in R (R Core Team 2016) to account for
188 expected variability in nutritive condition and EPRs by age and sex. Age and sex data were
189 available from long-term demographic modeling efforts (Center for Whale Research 2020). We
190 fit separate smooth terms to male and female EPRs from whales aged 0-60 (Figure 1). We used
191 the raw residuals (observed EPR minus mean EPR estimated by the spline fit) as the basis for
192 defining body condition classes. Ages of a few mature Southern Resident killer whale females
193 that were reproductive when monitoring began in the 1970s are not known precisely, so we
194 calculated residuals for those whales by subtracting observed EPRs from the mean EPR of
195 whales age 60+. We aggregated the residuals of all EPR measurements from all pods across all
196 years and split that distribution into five equal quantiles, representing the age- and sex-
197 normalized body condition classes to be used in the multi-state model, with body condition class
198 1 (BC1) being the lowest 20% quantile and BC5 being the highest 20% quantile. Finally, we
199 created a matrix of individuals' body condition classes by year, including unsampled years 2009-
200 2012 and 2014. In unsampled years, and in years where a whale was not photographed despite
201 survey effort, individual condition was logged as 'NA'. Known deaths from the annual census
202 (Center for Whale Research 2020) were also included in the matrix to facilitate estimation of
203 both age/sex- and body condition-specific mortality probabilities. Because photogrammetry data
204 were collected in September of each year, we considered deaths that occurred between October
205 and the following September to belong to the following survey year. For example, if a whale was
206 measured in September 2016, and died in November 2016, we logged that death in the following
207 time step of the condition matrix, 2017, to allow the model to account for the transition from the
208 condition measured in September 2016 to death. Two known anthropogenic-related deaths

209 (whales J34 and L95) were not included in the model, and the condition matrix for those whales
210 was left as unknown ('NA') after their last measurements, to prevent them from influencing
211 mortality probabilities for their respective body condition classes prior to death.
212
213 *Statistical model*
214 We developed a Bayesian multi-state modeling framework to evaluate changes in body condition
215 between years and the probability of mortality of different condition classes, after accounting for
216 differences in mortality by age and sex. All modeling was performed in JAGS via R (Plummer
217 2003) and built upon previous multi-state modeling approaches (Kery and Schaub 2012). The
218 model estimated annual transition probabilities between body condition classes, as well as
219 transitions from each body condition class to death, which are the condition-specific mortality
220 probabilities. An increase of one condition class (e.g. BC 1 to BC 2; BC 3 to BC 4) was
221 considered 'Growth' (G). Increases of two or more condition classes were considered multiple
222 single Growth steps and their probabilities were therefore exponentiated (e.g. BC 1 to BC 3 = G^2;
223 BC 1 to BC 4 = G^3). Remaining in the same condition class in two sequential years was
224 considered 'Stable' (S). A decrease of one condition class was considered 'Decline' (D) and
225 decreases of two of more condition classes were exponentiated as with Growth transitions. The
226 advantages of using power functions for the G and D elements are that the number of parameters
227 is reduced relative to an unconstrained matrix, and transitioning across multiple steps is
228 constrained to be less likely than transitioning a single step. In order to make population-level
229 inferences from individual changes in condition, all animals transitioning in the same direction
230 and magnitude contributed to the same transition probabilities, regardless of their starting
231 condition class:

$$
\begin{array}{cccccccc}
 & BC1 & BC2 & BC3 & BC4 & BC5 & Dead \\
BC1 & S_t & G_t & G_t^2 & G_t^3 & G_t^4 & M_{1_{i,t}} \\
BC2 & D_t & S_t & G_t & G_t^2 & G_t^3 & M_{2_{i,t}} \\
BC3 & D_t^2 & D_t & S_t & G_t & G_t^2 & M_{3_{i,t}} \\
BC4 & D_t^3 & D_t^2 & D_t & S_t & G_t & M_{4_{i,t}} \\
BC5 & D_t^4 & D_t^3 & D_t^2 & D_t & S_t & M_{5_{i,t}} \\
Dead & 0 & 0 & 0 & 0 & 0 & 1
\end{array}
$$

where rows are the condition class in year *t-1*, columns are the condition class in year *t*, and the matrix is populated by transition probabilities for year *t*. To make the sum of each row equal to 1, we normalized each row by dividing each element by its row sum (e.g. Cobb & Chen 2003; Liu et al. 2008). Mortality probabilities *M* were dependent on an individual whale's age, sex, and body condition. As a result, differences in mortality probability based on age, sex, and body condition slightly affected transition probabilities during row normalization. This can be interpreted as making transition probabilities between condition classes conditional upon a whale surviving.

Mortality probability was estimated in two steps: first based on the age and sex of a whale and then based on the condition class of that whale. We assigned an age class to each whale at each time step in the model, following previous classifications used for SRKW demographic modeling (Ward et al. 2013). Both males and females age 0-2 were defined as calves, and 2-10 as juveniles. Females age 10-44 were defined as young females and 44+ as old females. Males age 10-22 were defined as young males and 22+ as old males (Figure 1). The baseline mortality probability for whales in each age class was defined as:

$$M_{Base_a} \sim N[logit(\widehat{M}_{Base}), \sigma]$$

$$\widehat{M}_{Base} \sim U[0,1]$$

where M_{Base} is the baseline mortality probability for a whale in age class *a* (of the 6 age / sex classes defined above), which is normally distributed around the overall mean mortality probability, $\widehat{M}_{Base}$, with variance σ in logit space. We then added a random effect of body condition such that the mortality probability of a whale at a given time step was calculated as:

$$M_{i,t} = inv.logit(M_{Base_{i,t}} + M_{bc_{i,t}})$$

$$M_{bc} \sim N[0, \sigma]$$

where *M* is the mortality probability (in proportional space) for whale *i* at time *t*, M_{Base} is the age-specific baseline mortality probability (in logit space) for whale *i* given its age and sex class at time *t*, and M_{bc} is the condition-specific effect (in logit space) on baseline mortality for whale *i* given its body condition class *bc* at time *t*. M_{bc} for body condition class *bc* (1-5) is normally distributed around zero with variance σ in logit space. After applying the random effect of body condition to the whale's baseline mortality probability, that sum is converted to proportional space using the inverse logit transformation.

To incorporate salmon abundance covariates into the model we used a cumulative logit transformation to allow covariates to have independent relationships to Growth and Decline transition probabilities while remaining bounded by [0,1] in proportional space. For Growth and Decline transitions we used the following equation:

$$Transition_{c,t} = e^{intercept_c + slope_c * covariate_t + \varepsilon_{c,t}}$$

Where *Transition* is the uncorrected transition probability in cumulative logit space of transition type *c* (i.e. G or D) at time *t*, *intercept* and *slope* are the linear relationship terms for each transition type *c*, *covariate* is the salmon index at time *t*, and ε is the residual error around the linear fit for transition type *c* at time *t*, with

$$\varepsilon_{c,t} \sim N[0, \sigma]$$

where the ε terms for each transition type *c* are normally distributed around zero with variance σ. In the cumulative logit transformation, one parameter must be fixed at 1 for identifiability, which we applied to the probability of Stable condition (S):

$$Transition_{S,t} = 1$$

The uncorrected transition probabilities are then transformed to proportional space so that they are bounded by [0,1]:

$$Prob_{c,t} = \frac{Transition_{c,t}}{\sum_i Transition_t}$$

where *Prob* is the corrected probability for each transition type *c* (G, D, and S) at time *t*.

Salmon covariates

We evaluated 7 different Chinook salmon abundance indices to identify potential relationships between SRKW body condition and prey availability. We only considered Chinook salmon

297 given the reported importance of Chinook to SRKW life history and reproductive success (Ward
298 et al. 2009, Ford et al. 2010). We used estimates of Chinook salmon abundance from a model
299 used to manage salmon harvest (Fishery Regulation Assessment Model; FRAM) (Pacific Fishery
300 Management Council 2008). The FRAM model estimates the abundance of multiple west coast
301 salmon populations (or 'stocks') available to fisheries, and its outputs were recently synthesized
302 with Chinook spatio-temporal distribution models to generate indices of Chinook available to
303 killer whales by area, year, and season (Pacific Fishery Management Council 2020).
304
305 We used 3 stock-specific and 4 area-specific Chinook indices (Pacific Fishery Management
306 Council 2020). In this framework, estimates of Chinook are generated by season, corresponding
307 to the seasons in the FRAM model (Oct – Apr, May – Jun, Jul - Sep). For all analyses, we used
308 estimated starting abundances on July 1st of each year. SRKW are imaged in September each
309 year, so this summer index of abundance provides the closest match to the true prey availability
310 experienced by whales prior to condition measurements. Furthermore, condition at the time of
311 measurement is unlikely to represent the availability of prey more than a few months prior, as
312 SRKW condition is known to fluctuate seasonally, presumably in response to foraging
313 opportunities (Fearnbach et al. 2018). We focused on 3 of the larger stock-specific indices
314 (Fraser River, Columbia River, and Puget Sound), and included all modeled stock abundances
315 originating from those tributaries (Table S2). The 4 area-specific indices we used were North of
316 Cape Falcon (NOF), Oregon (OR), the Salish Sea (Salish), and Southwest Vancouver Island
317 (SWVI) (Pacific Fishery Management Council 2020). These area-specific indices summed the
318 model estimated abundances of all Chinook salmon from all index stocks that were estimated to
319 be present.

320

321 Transition probabilities within the model were related to the salmon index of the year that the
322 whales were transitioning into. For example, the probability of growth (G) from condition class
323 in September 2014 to condition class in September 2015 was linked to estimated Chinook
324 abundance on July 1st of 2015. Given the observed differences in body condition trends between
325 SRKW pods, we ran J, K, and L pods through the model separately, each with the same 7
326 candidate covariates to identify potential relationships between each pod and various salmon
327 indices. To determine whether there was support for the inclusion of covariates on transition
328 probabilities, we also considered a null model (condition transition probabilities fixed across all
329 years) and a time-only model (condition transition probabilities estimated independently each
330 year with no covariate. Given the relatively small number of deaths that occurred during the
331 study period, and previous studies that have assumed shared mortality probabilities across pods
332 (Ward et al. 2013), we also ran null and time-only models for all pods combined to estimate
333 population-wide mortality probabilities with body condition effects. For each model we ran 3
334 chains of 100,000 iterations each, with a burn-in of 50,000 iterations and thinning of 50 for a
335 total of 3,000 samples from the posterior distribution. We used non-informative uniform priors
336 for all parameters (Mitchell and Beauchamp 1988), and confirmed model convergence using
337 potential scale reduction factors (Gelman and Rubin 1992) (all parameters PSRF < 1.05) and
338 visual inspection of chain convergence.

339

340 *Model Selection*

341 To identify which (if any) Chinook salmon covariates best predicted SRKW body condition
342 transitions, we used a K-fold cross validation approach (Vehtari et al. 2017). There are many

343 different ways to split training and test data sets for cross validation, depending on the goals of
344 inference. Because our focus is on the temporal aspect, and in developing tools for making short
345 term future predictions of body condition, we treated data from each year iteratively as a 'fold'.
346 For each pod and covariate combination, we ran the multistate condition transition model once
347 with each year of observed condition data held out (n = 7 years), using the remaining years of
348 observed condition data to fit the estimated condition transition probabilities and covariate
349 relationships. We then calculated the expected log pointwise predictive density (ELPD) across
350 all held out years of observed body conditions based on the conditions in the previous year and
351 the model-estimated transition probabilities, following (Vehtari et al. 2017). We performed K-
352 fold Cross Validation for each of the pod and covariate combinations, as well as for each pod
353 with the null and time-only models described above. In addition to the computing the ELPD for
354 each model (models with the highest ELPD receive the highest data support), we calculated the
355 standard error – which is useful in quantifying the uncertainty associated with model selection
356 (Vehtari et al. 2017).
357
358 **Results**
359 In the 7 sampled years between 2008 and 2019, a total of 473 measurements of body condition
360 were collected from 99 whales, which were used in our analyses. We recorded a median of 5
361 years of body condition measurements for each whale (range 1-7). A total of 47 deaths and 33
362 births were documented in SRKWs between 2008 and 2019, while a total of 29 deaths and 15
363 births were documented in SRKWs during the same 7 years as the aerial photogrammetry
364 sampling (Center for Whale Research 2020).
365

366 In general. K-fold Cross Validation from our Bayesian models suggested that killer whale body
367 condition is better predicted when salmon covariates are included, relative to models without
368 salmon (J and L pods, Table S1). For models with salmon included, the standard errors of the
369 ELPD values exceeded the difference in ELPD values among candidate models, which makes it
370 challenging to confidently select one best-fit model. Consequently, we also report the second-
371 best fit model for each pod (Figures S1-S3). Due to the complexities of our model and the
372 number of parameters, we present both the raw estimated transition probabilities, as well as
373 aggregated Stable and Growth transition probabilities. This grouping represents a 'Positive'
374 transition group that may be more useful for managers targeted at preventing condition declines
375 and maintaining stable or increasing condition.
376
377 Fraser River Chinook was the best predictor of J pod condition transitions (Figure 2, Table S1),
378 although the ELPD values of the Salish Sea area-based Chinook abundance model fit (which
379 includes a large proportion of the Fraser River stock) was almost identical. J Pod had a
380 significant negative relationship between Fraser River Chinook abundance and the probability of
381 declining condition (Decline), with 95.3% of posterior draws for the slope term in the cumulative
382 logit regression < 0. There was no clear relationship between Fraser River Chinook abundance
383 and the probability of increasing condition (Growth) (38.5% of posterior draws > 0), and while
384 the probability of Stable condition appears to have a positive relationship with Fraser River
385 Chinook, a slope term for S is not explicitly calculated in the cumulative logit regression.
386 However, as the sum of the probabilities of Growth and Stable condition is equal to 1 minus the
387 probability of Decline, we can infer that there is a positive relationship between Fraser River
388 Chinook and Positive condition transitions (Growth or Stable condition) (Figure 2). When Fraser

River Chinook salmon abundance was above 750,000 fish, J pod whales had a greater than 0.86 median probability of stable or increasing condition. That probability decreased at lower Fraser River Chinook abundance, to a minimum 0.37 median probability of increasing or stable condition when Fraser River Chinook abundance fell to 347,000 fish.

The best fit model for L pod included Chinook Salmon from Puget Sound, and nearly all models with salmon included outperformed the null models (Table S1). There was moderate support for a negative relationship between Puget Sound Chinook abundance and the probability of declining condition, with 88% of posterior draws for the slope < 0. Similar to the results for J pod, there was no clear relationship between this index of salmon abundance and the probability of increasing condition (56.9% of posterior draws > 0). Nevertheless, when Puget Sound Chinook abundance was above 399,000 fish during the study period, L pod whales had a 0.82 – 0.89 median probability of stable or increasing condition. At the second-lowest Puget Sound Chinook abundance during the study period, 235,000 fish in 2015, L pod whales had a 0.32 median probability of stable or increasing condition. The major deviation from the positive linear relationship between Puget Sound Chinook abundance and condition transitions occurred in 2014, when Puget Sound Chinook was at its lowest point during the study period (208,000 fish), but L pod whales had a 0.60 median probability of stable or increasing condition. Apart from Puget Sound Chinook, all other models for L pod that included salmon covariates (both stock-specific and area-based abundance) produced potentially spurious results, where higher salmon abundance was associated with declining condition (e.g. Figure S3).

411 Unlike J and L pods, the best-fit model for K pod did not include salmon as a covariate, and
412 transition probabilities were held constant across years. In this null model, the median fixed
413 probability of increasing condition (Growth) was 0.40 (95% highest posterior density intervals
414 [HPDIs]: 0.33 – 0.47). The median probability of Decline was 0.31 (0.25 – 0.37), and the median
415 probability of Stable condition was 0.29 (0.21 – 0.38). The second best-fit model for K pod
416 included Puget Sound Chinook abundance, however we note that this covariate relationship
417 produced relatively constant condition transitions across years (Figure S2). Nevertheless, there
418 was a significant positive relationship between Puget Sound Chinook abundance and the
419 probability of increasing condition, with 94.93% of posterior draws for the slope > 0. There was
420 no clear relationship between Puget Sound Chinook abundance and the probability of declining
421 condition (22.6% of draws < 0), and the probability of stable condition decreased with increasing
422 Chinook abundance (Figure S2). When Puget Sound Chinook abundance was above 399,000
423 fish, K pod whales had a median 0.43 – 0.50 probability of increasing condition. In contrast,
424 when Puget Sound Chinook abundance was at a low of 208,000, K pod whales had a median
425 0.14 probability of increasing condition. However, the probability of the management-relevant
426 combined Growth and Stable condition remained relatively constant across the study period
427 (median 0.68 – 0.78 probability; Figure S2).
428
429 While observations of body condition provided a relatively large sample size for estimating
430 transition probabilities, deaths were relatively uncommon during the 12-year study period.
431 Consequently, we estimated the effects of age, sex and body condition on mortality probabilities
432 by pooling all pods together and running models without covariates (null and time-only). There
433 were 25 total deaths of whales that also had measurements of body condition in at least one year

434 during the study period (12 in J pod, 3 in K pod, and 10 in L pod). 15 of those deaths occurred in
435 the time step immediately following a body condition measurement. With data from all pods
436 combined, the null model had a higher ELPD score than the time only model (Table S1) and was
437 therefore used for estimates of mortality probability. The median expected mortality probabilities
438 for whales in each age/sex and body condition class are reported in Table 2. The expected
439 mortality probability of whales in body condition class 1 was 2-3 times higher than other body
440 condition classes (Figure 3, Table 2). Mortality probability decreased in condition class 2, was
441 lowest in condition classes 3 and 4, and increased slightly in condition class 5 to levels similar to
442 condition class 2. For example, based on the model estimates, a Young Female whale has
443 expected mortality probabilities of: BC1 0.03 (0.009-0.081); BC2 0.014 (0.003-0.043); BC3
444 0.009 (0.001-0.033); BC4 0.01 (0.001-0.033); BC5 0.017 (0.005-0.048). Of the whales that died
445 during the study period, condition class 1 whales died soonest after their final condition
446 measurement (mean 169 days), while the time between measurement and estimated death
447 roughly increased with condition class: mean 456, 790, 572, and 905 days for classes 2-5,
448 respectively (Figure 4).
449

450 **Discussion**

451 The Southern Resident killer whale population offers a unique study opportunity for individual-
452 based body condition monitoring, providing a robust framework that can be extended to other
453 marine and terrestrial populations. Due to the small population size, intensive demographic
454 monitoring, and known fates of virtually every individual, paired with annual photogrammetry
455 measurements of most of the population, we were able to make direct estimates of the
456 relationship between individual salmon stocks and SRKW condition, and relate condition to

457 survival probability. While small demographic fluctuations limit statistical power for identifying
458 the influence of covariates such as prey abundance, aerial photogrammetry allows for more
459 individuals to be sampled in each year and repeatedly sampled across years, increasing power to
460 evaluate changes in body condition against possible drivers. In this case, we obtained more than
461 ten times as many observations of body condition as observations of births and deaths in the
462 seven years of data collection. While our time series of condition measurements was relatively
463 short, we posit that with continued annual monitoring this method will provide sufficient
464 statistical power for even finer scale investigations of prey availability and population status (e.g.
465 at the individual stock level rather than tributary-level aggregates). Evaluating changes in body
466 condition over time likely provides more insights into drivers of population health than simply
467 comparing single measures of condition (e.g. annual population mean and variance) to potential
468 covariates, given the ability of long-lived animals such as killer whales to live through
469 bottlenecks in resource availability. In addition, there may be inherent differences in baseline
470 condition between individuals, so evaluating individual changes between years rather than raw
471 condition further accounts for individual variability.
472
473 Our cross-validation analyses suggest that, in the case of J and L pods, models including salmon
474 covariates better predicted held-out years of body condition data than models without salmon
475 covariates. Given that salmon managers use the FRAM model to generate pre-season estimates
476 of Chinook abundance by stock, the modeling framework we present here could be used to
477 generate predictions of fall SRKW body condition based on those salmon abundance estimates,
478 quantify short-term risks to the population, and identify potential management interventions. Our
479 model results suggest the strongest correlation between killer whale body condition and prey is

480 between the SRKW J pod and Chinook salmon returning to the Fraser River. The Salish Sea
481 area-based Chinook index was essentially tied for the best-fit J pod model, which is unsurprising
482 considering the Salish Sea index is typically made up of 40-50% Fraser-origin Chinook. Over the
483 last decade, when Fraser River Chinook abundance was above 750,000 (estimated FRAM
484 Chinook model abundance on July 1st), J pod whales had a low chance (less than 14%) of
485 declining body condition. Such a target could be used in a management setting to define
486 thresholds supporting the stability and recovery of this population segment. For example,
487 management actions focused on habitat restoration that ensures effective anadromous migration
488 and productivity of Fraser River Chinook stocks could lead to gains in the nutritive condition of J
489 pod whales. In the long-term, increasing urbanization of watersheds (Greene and Beechie 2004),
490 increasing abundance of competing predators (Chasco et al. 2017), and climate change (Crozier
491 et al. 2008) all present substantial threats to Fraser River Chinook abundance.
492
493 The only positive, ecologically plausible relationship we found for L pod body condition was
494 with the Puget Sound stock-specific abundance index. This is surprising, given that L pod is
495 rarely in Puget Sound in the summer and spends less time in adjacent inland waters during the
496 summer months than J or K pods (Riera et al. 2019), and Puget Sound origin Chinook are
497 generally smaller and less numerically dominant than other stocks (O'Neill et al. 2014, Pacific
498 Fishery Management Council 2020). However, L pod spends more time during the summer
499 months in the western strait of Juan de Fuca than J or K pods (Riera et al. 2019), and may be
500 targeting Puget Sound Chinook as they migrate from their open ocean phase towards spawning
501 tributaries. The somewhat unique oceanic distribution of Puget Sound Chinook along the west
502 coast of Vancouver Island (Weitkamp 2010, Shelton et al. 2019) may provide a reliable prey

503 base in areas or times when more dominant stocks (Columbia and Fraser rivers) are less
504 abundant. The relationship between L pod body condition transitions and Puget Sound Chinook
505 abundance was weaker than the relationship between J pod and Fraser River Chinook. It is
506 possible that L pod targets Chinook from a variety of stocks as they enter the strait of Juan de
507 Fuca, which could obscure the signal of the Puget Sound Chinook's influence on L pod body
508 condition. However, L pod body condition was negatively correlated to all other stock-specific
509 and area-based indices, including all Chinook salmon present in the Southwest Vancouver Island
510 region, which presumably would be a better representation of Chinook availability at the mouth
511 of the strait of Juan de Fuca. Previous analyses examining the influence of specific Chinook
512 stocks on SRKW demographic rates found a significant relationship between SRKW fecundity
513 and both Puget Sound and Fraser River Chinook abundance (Vélez-Espino et al. 2014), which
514 further indicates the potential importance of these stocks to the SRKW population.
515
516 The best-fit model for K pod had fixed body condition transition probabilities across time and
517 included no salmon covariate. K pod may forage on a diverse assemblage of prey that is not
518 easily captured in either stock-specific or area-based indices of Chinook abundance. However,
519 the second best-fit model for K pod included Puget Sound Chinook and suggested a positive
520 relationship between Chinook abundance and the probability of increasing body condition.
521 Additional studies of the fine scale distribution of Puget Sound Chinook along Vancouver Island
522 and the Washington coast, and their representation in the diets of L and K pod whales during
523 summer months could improve our understanding of the importance of this stock to SRKW
524 population health. The major caveat to our findings is that body condition is known to fluctuate
525 over a period of several months (Fearnbach et al. 2019). The three SRKW pods forage on other

526 salmon stocks in winter and spring months (Hanson et al. 2010), but the September body
527 condition metrics, and therefore the results of our analyses, most likely reflect the effects of the
528 summer foraging period in the Salish Sea.
529
530 In addition to demonstrating the link between salmon abundance and body condition of killer
531 whales, our model results show that whales in poor condition are more likely to die. Our
532 estimated baseline mortality rates of whales in different age and sex classes are generally in line
533 with previous findings (Ward et al. 2013), with old males and females experiencing the highest
534 mortality probabilities, and calves experiencing slightly elevated mortality probabilities
535 compared to juveniles and young whales. Our model estimated somewhat higher mortality
536 probabilities for old females, and lower for old males, calves, and juveniles than previous
537 analyses (Ward et al. 2013). These small differences are most likely due to the shorter time series
538 of deaths included in our study (2008-2019 versus 1979-2010) and the exclusion of whales that
539 did not have body condition measurements, although we cannot rule out changes in mortality
540 probability by age and sex class in recent years. Whales in condition class 1 had a mortality
541 probability roughly 2-3 times higher than whales in condition classes 2-5. Interestingly,
542 condition class 5 whales had a slightly elevated mortality probability similar to condition class 2
543 whales. The two whales that were observed in condition class 5 at the time step immediately
544 prior to death died 317 (L53) and 349 (J14) days after being imaged, and may have experienced
545 a substantial, unrecorded decline in condition during that almost year-long period. Furthermore,
546 while we did account for age and sex effects on mortality probability, there are other factors
547 aside from age, sex, and nutritive condition that may contribute to mortality probabilities, such as
548 the presence or condition of other whales in a matriline (Foster et al. 2012, Nattrass et al. 2019).

549 The majority of whales that died shortly after being imaged were in condition class 1 (very poor
550 condition), while deaths of higher condition class whales typically occurred longer after their last
551 measurement (Figure 4). This further supports the conclusion that whales in condition class 1
552 have an elevated mortality probability and suggests that aerial photogrammetry measurements
553 may be able to identify whales most at risk of death in the near future.
554
555 Interestingly, changes in condition for animals from J and L pod were best explained by Chinook
556 indices that are negatively correlated with one another (Figure S4), while K pod condition was
557 best explained by constant transition probabilities (or possibly Puget Sound Chinook, similar to
558 L pod). Our findings suggest that the three pods behave very differently in terms of body
559 condition fluctuations, which are likely driven by independent foraging strategies. Recent
560 analyses of SRKW demographic data attempted to relate births and deaths to a wide range of
561 Chinook salmon area-based indices (including several of the area-based indices used in this
562 study), but found no significant relationships (Pacific Fishery Management Council 2020). Our
563 results indicate that it may be advantageous for similar future analyses of demographic
564 fluctuations to consider the three SRKW pods separately. Furthermore, given the differences in
565 important prey indices reported here, it may be more effective for management strategies to treat
566 the population of SRKWs as multiple management units, as the most effective management
567 actions would likely be very different for each pod based on our findings.
568
569 In addition to identifying target prey abundance levels to support SRKW recovery, aerial
570 photogrammetry can provide an early warning system that has the potential to serve as the basis
571 for dynamic and adaptive management strategies. In an endangered population that had only 73

572 remaining individuals as of 2019, demographic casualties such as the death of a reproductive
573 female or a year with no successful births can potentially have catastrophic consequences for
574 population viability. Management actions that respond to these demographic casualties as
575 opposed to preventing them may be insufficient to support population recovery. Our findings
576 show that aerial photogrammetry can be used to identify at-risk individual whales, as well as to
577 collect an overall metric of population health prior to mortality events that could be used to
578 inform management actions. For example, if a large portion of the population is recorded in body
579 condition class 1 during September (e.g. more than 20% of the population, or some threshold
580 decided upon by managers), then fishery actions could be considered to increase prey availability
581 for SRKW pods over the next year. Some actions that may result in an increase in Fraser
582 Chinook abundances include spatio-temporal closures in areas of high Fraser Chinook encounter
583 rates or mark-selective regulations, as a high proportion of the Fraser stock aggregate is
584 unmarked. However, we note that the predicted fishing mortalities on Chinook are thought to be
585 relatively low compared to the total cohort size (Pacific Fishery Management Council 2020) and
586 that proactive strategies to increase Chinook abundance such as habitat restoration, reducing
587 predator-related mortality, and increased production may provide the greatest benefit to overall
588 Chinook abundance (Greene and Beechie 2004, Crozier et al. 2008, Chasco et al. 2017). These
589 approaches could be implemented at the pod level where, for example, if individuals from K and
590 L pods are in good condition while J pod individuals are in poor condition, management action
591 could be taken to increase Fraser River Chinook availability over the coming year. These
592 assessments of condition could be done in near-real time with a lag of less than 3 months, rapidly
593 informing upcoming management strategies or allowing for interventions at the individual level.
594 In addition to influencing survivorship, body condition is likely also tied to fecundity in killer

595 whales (Ward et al. 2009). Future work should examine the relationship between reproductive
596 success in the SRKW population and observed body condition, which would allow for a full
597 evaluation of the influence of individual condition on overall population viability and support
598 further modeling and projection efforts to weigh the efficacy of candidate management
599 strategies. In addition, monitoring body condition in other seasons could provide insights into
600 prey populations that may be important to the SRKW population in winter and spring months.
601 As the time series of condition measurements grows it may be possible to evaluate the
602 relationship between SRKW condition and finer scale Chinook stock groupings and potentially
603 other prey species.
604
605 It may not be possible to apply the approach used in this study to larger, wide ranging
606 populations of marine mammals where repeated measurements of individuals and samples from
607 a large portion of the population are not feasible. Instead, the average body condition of a
608 random sample of the population may be achievable and, based on our findings, can likely serve
609 as a proxy for short-term, relative population health. In addition, we posit that rapid changes in
610 average body condition within a population can be used as an early-warning indicator of
611 upcoming demographic fluctuations, given our findings that individuals in poor conditions have
612 higher mortality probabilities. The use of body condition as an indicator of population health
613 could be further tested in cetacean populations that have long-term photogrammetry datasets and
614 experience substantial population fluctuations, such as eastern north Pacific gray whales
615 (Perryman and Lynn 2002), validating its use as a preceding signal of demographic impacts and
616 supporting the development of adaptive management strategies.
617

Acknowledgements

Aerial and boat-based operations around whales were conducted under the authority of National Marine Fisheries Service Permits 532-1822, 16163 and 19091 in US waters and Species-At-Risk Act Permit 13-278 in Canada. Field operations and data analysis were conducted with funding support from the National Fish and Wildlife Foundation, the National Oceanographic and Atmospheric Administration (NOAA), the U.S. Fish and Wildlife Service, Shell, SeaWorld, SR3, NOAA Office of Marine and Aviation Operations (OMAO), NOAA/NMFS Office of Science and Technology, the Ocean Wise Conservation Association and the SeaWorld and Busch Gardens Conservation Fund. We are thankful to Lynne Barre for her support and encouragement and to Chris Yates and Lisa Ballance for their role in acquiring NOAA funds to support analysis. We are also grateful to Ken Balcomb, Dave Ellifrit, Jane and Tom Cogan, Mark Malleson, Jessica Farrer and Dylan Jones for their assistance with field operations, Molly Groskreutz and Alyssa Paredes for their efforts with photogrammetry analysis, and Wayne Perryman, Don LeRoi, and the NOAA/OMAO Aircraft Operations Center for their support for drone flight operations. This research was performed while JDS held an NRC Research Associateship award at the NOAA Southwest Fisheries Science Center. The views and conclusions contained in this document are those of the authors and should not be interpreted as representing the opinions of policies of the U.S. Government or the National Fish and Wildlife Foundation and its funding sources. Mention of trade names or commercial products does not constitute their endorsement by the U.S. Government, or the National Fish and Wildlife Foundation or its funding sources.

641
642 **Literature Cited**
643

644 Berger, J. 2012. Estimation of Body-Size Traits by Photogrammetry in Large Mammals to
645 Inform Conservation. Conservation Biology 26:769–777.
646 Boulanger, J., M. Cattet, S. E. Nielsen, G. Stenhouse, and J. Cranston. 2013. Use of multi-state
647 models to explore relationships between changes in body condition, habitat and survival of
648 grizzly bears *Ursus arctos horribilis*. Wildlife Biology 19:274–288.
649 Brosi, B. J., and E. G. Biber. 2009. Statistical inference, type II error, and decision making under
650 the US endangered species act. Frontiers in Ecology and the Environment 7:487–494.
651 Center for Whale Research. 2020. Orca ID Guide: J,K, L Pod – Southern Resident Killer
652 Whales.
653 Chasco, B., I. C. Kaplan, A. Thomas, A. Acevedo-Gutiérrez, D. Noren, M. J. Ford, M. B.
654 Hanson, J. Scordino, S. Jeffries, S. Pearson, K. N. Marshall, and E. J. Ward. 2017.
655 Estimates of Chinook salmon consumption in Washington State inland waters by four
656 marine mammal predators from 1970 to 2015. Canadian Journal of Fisheries and Aquatic
657 Sciences 74:1173–1194.
658 Christiansen, F., A. M. Dujon, K. R. Sprogis, J. P. Y. Arnould, and L. Bejder. 2016. Noninvasive
659 unmanned aerial vehicle provides estimates of the energetic cost of reproduction in
660 humpback whales 7:1–18.
661 Christiansen, F., F. Vivier, C. Charlton, R. Ward, A. Amerson, S. Burnell, and L. Bejder. 2018.
662 Maternal body size and condition determine calf growth rates in Southern right whales.
663 Marine Ecology Progress Series 592:267–282.
664 Cobb, G. W., and Y.-P. Chen. 2003. An Application of Markov Chain Monte Carlo to
665 Community Ecology. The American Mathematical Monthly 110:265–288.
666 Crozier, L. G., R. W. Zabel, and A. F. Hamlet. 2008. Predicting differential effects of climate
667 change at the population level with life-cycle models of spring Chinook salmon. Global
668 Change Biology 14:236–249.
669 Dennis, B. 1989. Allee effects: Population growth, critical density, and the chance of extinction.
670 Natural Resource Modeling 3:481–538.
671 Durban, J. W., H. Fearnbach, W. L. Perryman, and D. J. Leroi. 2015. Photogrammetry of killer
672 whales using a small hexacopter launched at sea. Journal of Unmanned Vehicle Systems
673 3:131–135.
674 Fearnbach, H., J. Durban, D. Ellifrit, and K. Balcomb. 2018. Using aerial photogrammetry to
675 detect changes in body condition of endangered southern resident killer whales. Endangered
676 Species Research 35:175–180.
677 Fearnbach, H., J. W. Durban, L. G. Barrett-Lennard, D. K. Ellifrit, and K. C. Balcomb. 2019.
678 Evaluating the power of photogrammetry for monitoring killer whale body condition.
679 Marine Mammal Science:1–6.
680 Fearnbach, H., J. W. Durban, D. K. Ellifrit, and K. C. Balcomb. 2011. Size and long-term growth
681 trends of endangered fish-eating killer whales. Endangered Species Research 13:173–180.
682 Ford, J. K. B., G. M. Ellis, L. G. Barrett-Lennard, A. B. Morton, R. S. Palm, and K. C. Balcomb.
683 1998. Dietary specialization in two sympatric populations of killer whales (Orcinus orca) in
684 coastal British Columbia and adjacent waters. Canadian Journal of Zoology 76:1456–1471.
685 Ford, J. K. B., G. M. Ellis, P. F. Olesiuk, and K. C. Balcomb. 2010. Linking killer whale survival
686 and prey abundance: food limitation in the oceans' apex predator? Biology Letters 6:139–

142.
Ford, M. J., J. Hempelmann, M. B. Hanson, K. L. Ayres, R. W. Baird, C. K. Emmons, J. I. Lundin, G. S. Schorr, S. K. Wasser, and L. K. Park. 2016. Estimation of a killer whale (Orcinus orca) population's diet using sequencing analysis of DNA from feces. PLoS ONE 11:1–14.
Foster, E. A., D. W. Franks, S. Mazzi, S. K. Darden, K. C. Balcomb, J. K. B. Ford, and D. P. Croft. 2012. Adaptive prolonged postreproductive life span in killer whales. Science 337:1313.
Gelman, A., and D. B. Rubin. 1992. Inference from Iterative Simulation Using Multiple Sequences. Statistical Science 7:457–472.
Greene, C. M., and T. J. Beechie. 2004. Consequences of potential density-dependent mechanisms on recovery of ocean-type chinook salmon (Oncorhynchus tshawytscha). Canadian Journal of Fisheries and Aquatic Sciences 61:590–602.
Groskreutz, M., J. Durban, H. Fearnbach, L. Barrett-Lennard, J. Towers, and J. Ford. 2019. Decadal changes in adult size of salmon-eating killer whales in the eastern North Pacific. Endangered Species Research 40:183–188.
Hanson, M. B., R. W. Baird, J. K. B. Ford, J. Hempelmann-Halos, D. M. Van Doornik, J. R. Candy, C. K. Emmons, G. S. Schorr, B. Gisborne, K. L. Ayres, S. K. Wasser, K. C. Balcomb, K. Balcomb-Bartok, J. G. Sneva, and M. J. Ford. 2010. Species and stock identification of prey consumed by endangered southern resident killer whales in their summer range. Endangered Species Research 11:69–82.
Hu, J., X. Wu, and M. Dai. 2020. Estimating the population size of migrating tibetan antelopes pantholops hodgsonii with unmanned aerial vehicles. Oryx 54:101–109.
Kery, M., and M. Schaub. 2012. Bayesian Population Analysis using WinBUGS: A hierarchical perspective. Elsevier Inc.
Krahn, M. M., M. B. Hanson, G. S. Schorr, C. K. Emmons, D. G. Burrows, J. L. Bolton, R. W. Baird, and G. M. Ylitalo. 2009. Effects of age, sex and reproductive status on persistent organic pollutant concentrations in "Southern Resident" killer whales. Marine Pollution Bulletin 58:1522–1529.
Liu, D., K. Song, J. R. G. Townshend, and P. Gong. 2008. Using local transition probability models in Markov random fields for forest change detection. Remote Sensing of Environment 112:2222–2231.
Lusseau, D., D. E. Bain, R. Williams, and J. C. Smith. 2009. Vessel traffic disrupts the foraging behavior of southern resident killer whales Orcinus orca. Endangered Species Research 6:211–221.
Mitchell, T. J., and J. J. Beauchamp. 1988. Bayesian variable selection in linear regression. Journal of the American Statistical Association 83:1023–1032.
Nattrass, S., D. P. Croft, S. Ellis, M. A. Cant, M. N. Weiss, B. M. Wright, E. Stredulinsky, T. Doniol-valcroze, J. K. B. Ford, K. C. Balcomb, and D. W. Franks. 2019. Postreproductive killer whale grandmothers improve the survival of their grandoffspring:1–5.
O'Neill, S. M., G. M. Ylitalo, and J. E. West. 2014. Energy content of Pacific salmon as prey of northern and southern resident killer whales. Endangered Species Research 25:265–281.
Pacific Fishery Management Council. 2008. Fishery Regulation Assessment Model (FRAM) - An Overview for Coho and Chinook - v 3.0. Portland, Oregon.
Pacific Fishery Management Council. 2020. Pacific Fishery Management Council Salmon Fishery Management Plan Impacts to Southern Resident Killer Whales.

Parsons, K. M., K. C. Balcomb, J. K. B. Ford, and J. W. Durban. 2009. The social dynamics of southern resident killer whales and conservation implications for this endangered population. Animal Behaviour 77:963–971.

Perryman, W., M. E. Goebel, N. Ash, D. Leroi, and S. Gardner. 2014. Small Unmanned Aerial Systems for Estimating Abundance of Krill-Dependent Predators: a Feasibility Study with Preliminary Results. U.S. Antarctic Marine Living Resources Program. 2010/11 Field Season Report:64–73.

Perryman, W. L., and M. S. Lynn. 2002. Evaluation of nutritive condition and reproductive status of migrating gray whales (Eschrichtius robustus) based on analysis of photogrammetric data. Journal of Cetacean Research and Management 4:155–164.

Plummer, M. 2003. JAGS: A program for analysis of Bayesian graphical models using Gibbs sampling. Proceedings of the 3rd international workshop on distributed statistical computing 124.

R Core Team. 2016. R: A language and environment for statistical computing. R Foundation for Statistical Computing, Vienna, Austria.

Riera, A., J. F. Pilkington, J. K. B. Ford, E. H. Stredulinsky, and N. R. Chapman. 2019. Passive acoustic monitoring off Vancouver Island reveals extensive use by at-risk Resident killer whale (Orcinus orca) populations. Endangered Species Research 39:221–234.

Ruckelshaus, M. H., P. Levin, J. B. Johnson, and P. M. Kareiva. 2002. The Pacific salmon wars: What science brings to the challenge of recovering species. Annual Review of Ecology and Systematics 33:665–706.

Schönbrodt, F. D., and M. Perugini. 2013. At what sample size do correlations stabilize? Journal of Research in Personality 47:609–612.

Service, N. M. F. 2019. Killer Whale (Orcinus orca): Eastern North Pacific Southern Resident Stock. NOAA Marine Mammal Stock Assessment.

Sheer, M. B., and E. A. Steel. 2006. Lost Watersheds: Barriers, Aquatic Habitat Connectivity, and Salmon Persistence in the Willamette and Lower Columbia River Basins. Transactions of the American Fisheries Society 135:1654–1669.

Shelton, A. O., W. H. Satterthwaite, E. J. Ward, B. E. Feist, and B. Burke. 2019. Using hierarchical models to estimate stock-specific and seasonal variation in ocean distribution, survivorship, and aggregate abundance of fall run chinook salmon. Canadian Journal of Fisheries and Aquatic Sciences 76:95–108.

Soulé, M. E., editor. 1987. Viable populations for conservation. Cambridge University Press.

Vehtari, A., A. Gelman, and J. Gabry. 2017. Practical Bayesian model evaluation using leave-one-out cross-validation and WAIC. Statistics and Computing 27:1413–1432.

Vélez-Espino, L. A., J. K. B. Ford, H. A. Araujo, G. Ellis, C. K. Parken, and R. Sharma. 2014. Relative importance of chinook salmon abundance on resident killer whale population growth and viability. Aquatic Conservation: Marine and Freshwater Ecosystems 25:756–780.

Vindenes, Y., E. Edeline, J. Ohlberger, Ø. Langangen, I. J. Winfield, N. C. Stenseth, and L. Asbjørn Vøllestad. 2014. Effects of climate change on trait-based dynamics of a top predator in freshwater ecosystems. American Naturalist 183:243–256.

Walsh, P. D. 2000. Sample size for the diagnosis of conservation units. Conservation Biology 14:1533–1537.

Ward, E. J., M. J. Ford, Kope Robert G., J. K. B. Ford, L. A. Velez-Espino, C. K. Parken, L. W. LaVoy, M. B. Hanson, and K. C. Balcomb. 2013. Estimating the impacts of Chinook

salmon abundance and prey removal by ocean fishing on Southern Resident killer whale population dynamics. Page U.S. Dept. Commer., NOAA Tech. Memo. NMFS-NWFSC-123.

Ward, E. J., E. E. Holmes, and K. C. Balcomb. 2009. Quantifying the effects of prey abundance on killer whale reproduction. Journal of Applied Ecology 46:632–640.

Weitkamp, L. A. 2010. Marine Distributions of Chinook Salmon from the West Coast of North America Determined by Coded Wire Tag Recoveries. Transactions of the American Fisheries Society 139:147–170.

Wood, S. N. 2006. Generalized additive models: an introduction with R. Chapman and Hall, Boca Raton Fl.

Author Contributions:

JDS: Analysis conceptualization, data analysis, manuscript writing & editing

JWD: Study conceptualization, funding acquisition, data collection & analysis, manuscript editing

HF: Study conceptualization, funding acquisition, data collection & analysis, manuscript editing

LGBL: Funding acquisition, data collection, manuscript editing

PKC: Data analysis, manuscript editing

EJW: Data analysis, manuscript editing

DRD: Data analysis, manuscript editing

Data Availability:

Data and code to run multi-state models can be found at: https://github.com/stewart6/SRKW-MultiState

806 **Tables and Figures**

807

808 Table 1. Number of Southern Resident killer whales measured using aerial photogrammetry in
809 September of each study year, and the percentage of each pod imaged in parentheses.

810

Year	J Pod	K Pod	L Pod
2008	23 (92.0%)	18 (94.7%)	19 (46.3%)
2013	25 (96.2%)	18 (94.7%)	25 (67.6%)
2015	27 (100%)	19 (100%)	26 (74.3%)
2016	28 (96.6%)	19 (100%)	35 (100%)
2017	22 (91.7%)	9 (50.0%)	30 (85.7%)
2018	23 (100%)	18 (100%)	29 (85.3%)
2019	22 (100%)	17 (100%)	21 (61.8%)

811

812

813

814 Table 2. Model-estimated mortality probabilities by body condition (BC) and age/sex class for
815 Southern Resident killer whales. Reported values are median estimates with 95% highest
816 posterior density intervals in parentheses.

817

Age/Sex Class	BC 1	BC 2	BC 3	BC 4	BC 5
Calf	0.04 (0.004-0.177)	0.02 (0.001-0.085)	0.01 (0.001-0.066)	0.01 (0.001-0.069)	0.02 (0.002-0.105)
Juvenile	0.02 (0.003-0.060)	0.01 (0.001-0.030)	0.01 (0.000-0.025)	0.01 (0.000-0.025)	0.01 (0.002-0.037)
Young Female	0.03 (0.009-0.081)	0.01 (0.003-0.043)	0.01 (0.001-0.033)	0.01 (0.001-0.033)	0.02 (0.005-0.048)
Old Female	0.23 (0.069-0.595)	0.12 (0.026-0.348)	0.08 (0.010-0.261)	0.09 (0.011-0.274)	0.14 (0.042-0.406)
Young Male	0.03 (0.006-0.105)	0.01 (0.002-0.052)	0.01 (0.001-0.039)	0.01 (0.001-0.041)	0.02 (0.003-0.062)
Old Male	0.16 (0.047-0.432)	0.08 (0.018-0.231)	0.05 (0.006-0.171)	0.06 (0.007-0.173)	0.09 (0.026-0.267)

818

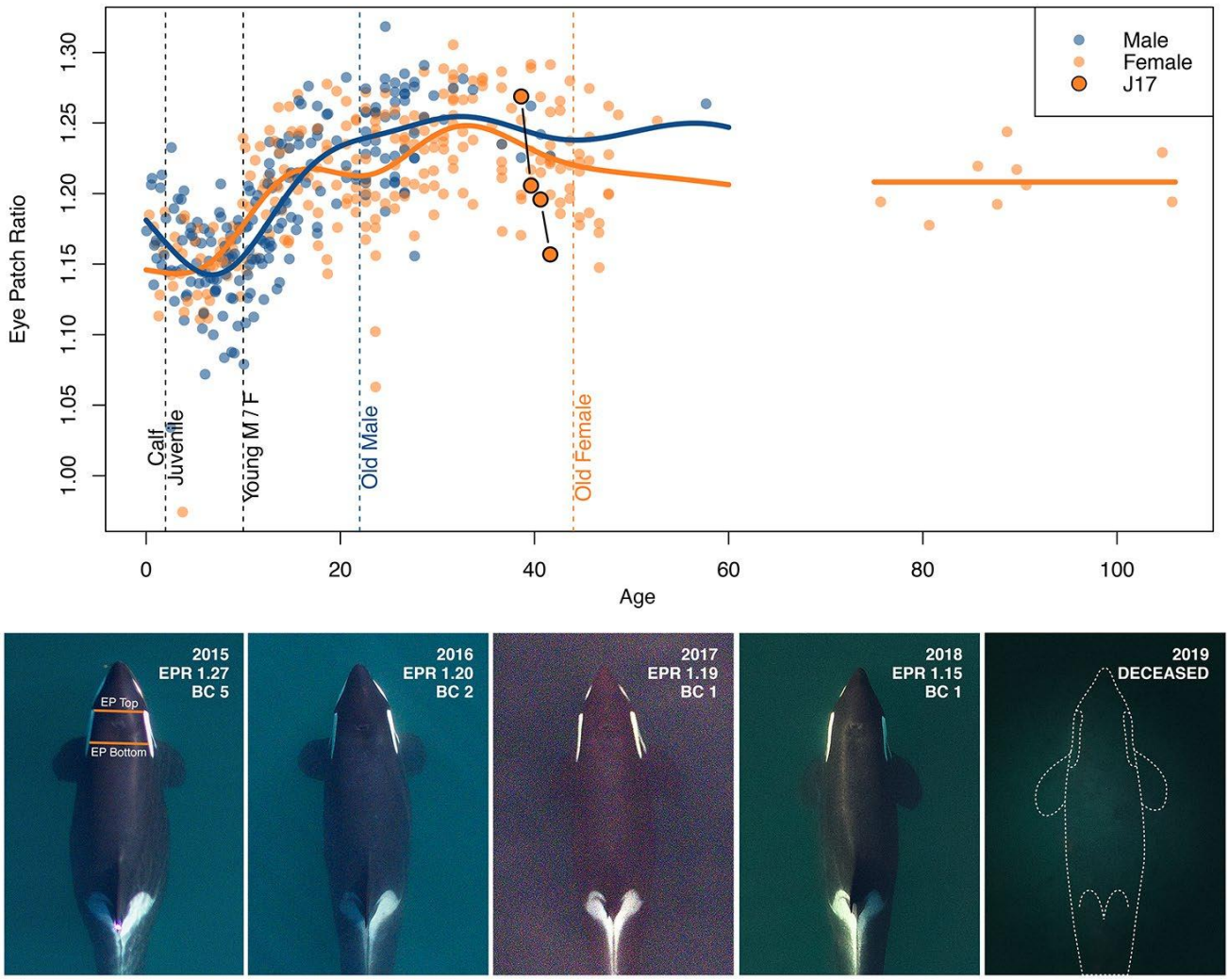

Figure 1. Eye patch ratios by age and sex for Southern Resident killer whale individuals from all three pods during the study period. The top panel shows the measured eye patch ratio by age for males (blue) and females (orange). The spline fits for males (blue) and females (orange) were used to define body condition classes based on residuals, while a mean Eye patch ratio was used to calculate residuals for females aged 60+ that did not have reliable age estimates (see Methods) Vertical dashed lines delineate the age and sex classes used to estimate age- and sex-specific mortality probabilities. The series of images tracks the eye patch ratio (EPR) and body condition class (BC) of adult female J17 from 2015-2018, demonstrating the observed decline in condition preceding her death in summer 2019. The progression of J17's eye patch ratios are highlighted in the top panel in larger, dark orange circles connected by lines. The orange horizontal lines in the far-left image show how the eye patch ratio is calculated (EP bottom divided by EP top), providing a metric of adipose fat behind the cranium as a proxy for nutritive condition.

Figure 2. Body condition transition probabilities for Southern Resident killer whale J (a-d) and L (e-h) pods with best-fit Chinook salmon covariates (Fraser River and Puget Sound, respectively). The best-fit model for K pod did not include a covariate (see Results). Panels show the model-estimated relationships between Chinook salmon abundance and the probability of a Decline in body condition (a,e), and the combined probability of Growth or Stable body condition (b,f). The probability of Growth or Stable condition shown in b & f is the sum of the posterior distributions for the probability of Growth (c,g) and the probability of Stable condition (d,h). Put simply, b = c+d and f = g+h. Points and vertical bars represent the median estimated transition probability with 95% Highest Posterior Density Intervals. The light and dark shading represent the 95% and 50% HPDIs, respectively, of the model-estimated relationship between salmon covariates and transition probabilities, along with the median estimate of this fit (black line).

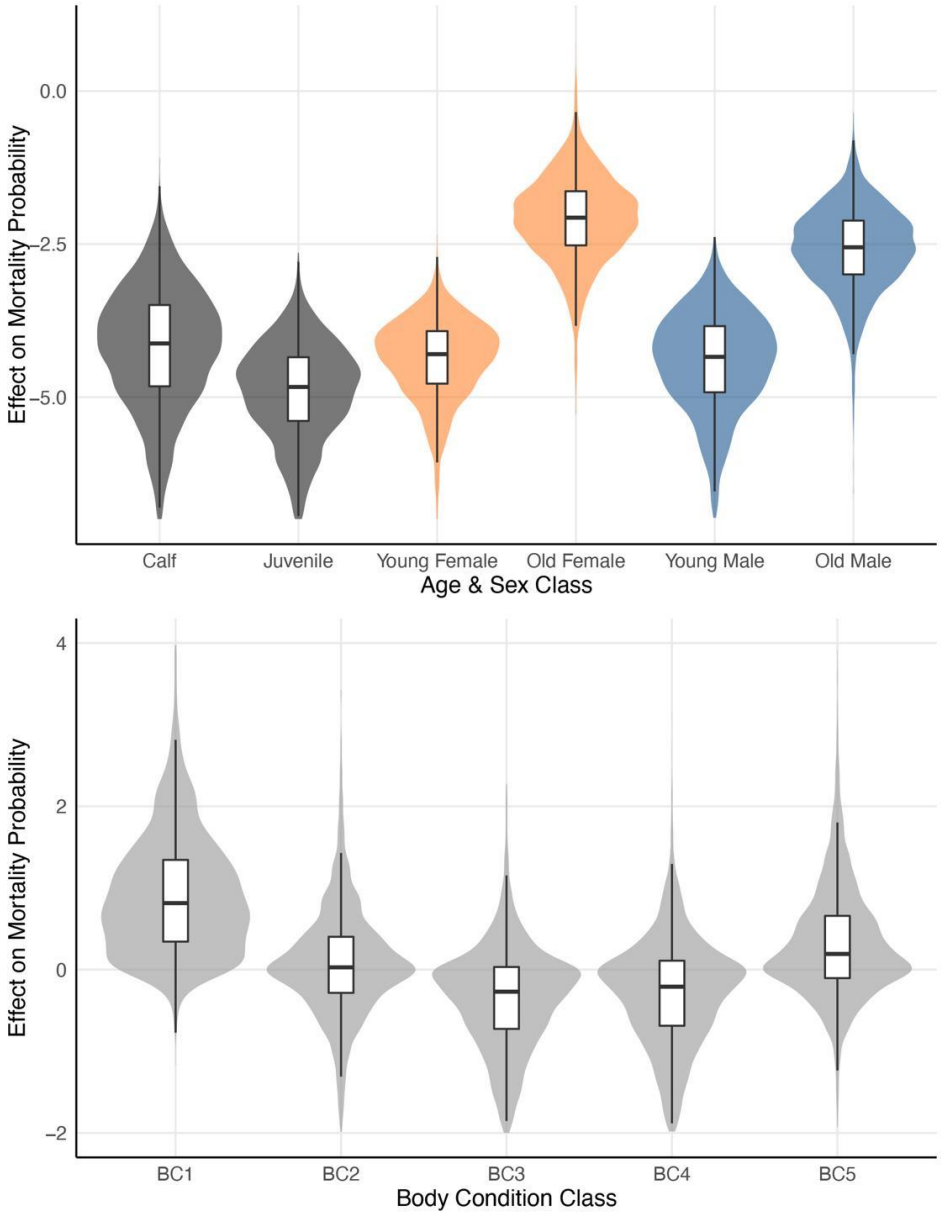

Figure 3. Age/sex class- and condition-specific mortality probabilities for Southern Resident killer whales (all pods combined). Calf and Juvenile age classes include both sexes. Violin plots represent the posterior distributions of the effect of age/sex (top) or body condition (bottom) class on mortality probability. Inset boxplots represent the median (black horizontal bar), 50% HPDI (white box), and 95% HPDI (vertical black lines). Note that the effects are applied in logit space before transformation to proportional space. See Table 2 for expected mortality probabilities of each age/sex and body condition class combination.

Figure 4. Time between final condition measurement and estimated death for Southern Resident killer whales that died during the 2008-2019 study period. Each density plot represents the estimated number of days between when a whale was last measured and when it died, broken out by the condition class (BC1-5) that whales were last recorded as before death. Points represent the time between final measurement and death for individual whales, color coded by pod and jittered randomly on the y axis.

Supplementary Information

Table S1. K-fold Cross Validation model selection table. Expected log pointwise predictive density (ELPD) scores with standard errors for all candidate Chinook salmon abundance indices as well as null and time only models for each Southern Resident killer whale pod. Fraser River, Columbia River, and Puget Sound are stock-specific abundance indices, while North of Cape Falcon, Oregon coast, Salish Sea, and Southwest Vancouver Island are area-based Chinook abundance indices. The null model holds transition probabilities constant across years, while the time only model estimates independent annual transition probabilities without the inclusion of a covariate. Null and time only models were also run for all pods combined to estimate a joint mortality probability based on age, sex, and body condition effects. (*) indicate the top two models based on ELPD scores for each pod. Bold values indicate the top model for each pod that is reported in the main text.

Covariate	**J Pod ELPD (SE)**	**K Pod ELPD (SE)**	**L Pod ELPD (SE)**	**All Pods ELPD (SE)**
Fraser River	**-188.92 (13.12)***	-106.11 (11.01)	-182.7 (19.07)	
Columbia River	-190.86 (12.82)	-109.77 (11.58)	-181.53 (19.4)	
Puget Sound	-191.18 (12.52)	-103.73 (10.39)*	**-178.66 (18.61)***	
North of Cape Falcon	-194.47 (12.79)	-111.36 (11.97)	-179.22 (19.16)*	
Oregon Coast	-192.44 (12.66)	-108.57 (11.32)	-179.57 (19.43)	
Salish Sea	-188.94 (13.25)*	-107.96 (10.95)	-183.78 (19.17)	
Southwest Vancouver Is.	-193.32 (12.94)	-113.55 (12.79)	-181.34 (18.96)	
Time Only	-195.89 (12.42)	-111.59 (12.38)	-182.55 (19.09)	-602.55 (32.66)
Null	-190.42 (13.31)	**-102.18 (11.32)***	-191.97 (24.24)	**-594.86 (31.79)**

899 Table S2. Chinook salmon stock-specific designations. All summer and fall stocks originating
900 within each tributary were aggregated into a single stock-specific abundance index. Each
901 stock is associated with a FRAM Stock Number and Stock Name.
902

Present Study Stock Assignment	FRAM Stock Number	Stock Name
Columbia River	37	UnMarked CR Oregon Hatchery Tule
	38	Marked CR Oregon Hatchery Tule
	39	UnMarked CR Washington Hatchery Tule
	40	Marked CR Washington Hatchery Tule
	41	UnMarked Lower Columbia River Wild
	42	Marked Lower Columbia River Wild
	43	UnMarked CR Bonneville Pool Hatchery
	44	Marked CR Bonneville Pool Hatchery
	45	UnMarked Columbia R Upriver Summer
	46	Marked Columbia R Upriver Summer
	47	UnMarked Columbia R Upriver Bright
	48	Marked Columbia R Upriver Bright
	53	UnMarked Snake River Fall
	54	Marked Snake River Fall
	67	UnMarked Lower Columbia Naturals
Fraser River	59	UnMarked Fraser River Late
	60	Marked Fraser River Late
	61	UnMarked Fraser River Early
	62	Marked Fraser River Early
Puget Sound	1	UnMarked Nooksack/Samish Fall
	2	Marked Nooksack/Samish Fall
	7	UnMarked Skagit Summer/Fall Fing
	8	Marked Skagit Summer/Fall Fing
	9	UnMarked Skagit Summer/Fall Year
	13	UnMarked Snohomish Fall Fing
	14	Marked Snohomish Fall Fing
	15	UnMarked Snohomish Fall Year
	16	Marked Snohomish Fall Year
	17	UnMarked Stillaguamish Fall Fing
	18	Marked Stillaguamish Fall Fing
	19	UnMarked Tulalip Fall Fing
	20	Marked Tulalip Fall Fing
	21	UnMarked Mid PS Fall Fing
	22	Marked Mid PS Fall Fing
	23	UnMarked UW Accelerated
	24	Marked UW Accelerated
	25	UnMarked South Puget Sound Fall Fing
	26	Marked South Puget Sound Fall Fing
	27	UnMarked South Puget Sound Fall Year
	28	Marked South Puget Sound Fall Year

710

Figure S1. Covariate relationships for Southern Resident killer whale J Pod & Salish Sea Chinook salmon (second best-fit model): Decline (D), Growth / Stable (G/S), Growth (G), Stable (S). Note that the probability of Growth or Stable condition in the top right panel is the sum of the posterior distributions of the probabilities of Growth (bottom left) and Stable condition (bottom right). Put simply, P(GS) = P(G) + P(S). Points and vertical bars represent the median estimated transition probability with 95% Highest Posterior Density Intervals, and the light and dark shading represent the 95% and 50% HPDI, respectively, of the model-estimated relationship between the Salish Sea Chinook abundance and transition probabilities, along with the median estimate of this fit (black line).

185 [redacted]

Figure S2. Covariate relationships for Southern Resident killer whale K Pod & Puget Sound Chinook salmon (second best-fit model): Decline (D), Growth / Stable (G/S), Growth (G), Stable (S). Note that the probability of Growth or Stable condition in the top right panel is the sum of the posterior distributions of the probabilities of Growth (bottom left) and Stable condition (bottom right). Put simply, P(GS) = P(G) + P(S). Points and vertical bars represent the median estimated transition probability with 95% Highest Posterior Density Intervals, and the light and dark shading represent the 95% and 50% HPDI, respectively, of the model-estimated relationship between the Puget Sound Chinook abundance and transition probabilities, along with the median estimate of this fit (black line).

[redacted] 1,510

Figure S3. Covariate relationships for Southern Resident killer whale K Pod & North of Cape Falcon (NOF) Chinook salmon (second best-fit model): Decline (D), Growth / Stable (G/S), Growth (G), Stable (S). Note that the probability of Growth or Stable condition in the top right panel is the sum of the posterior distributions of the probabilities of Growth (bottom left) and Stable condition (bottom right). Put simply, P(GS) = P(G) + P(S). Points and vertical bars represent the median estimated transition probability with 95% Highest Posterior Density Intervals, and the light and dark shading represent the 95% and 50% HPDI, respectively, of the model-estimated relationship between the NOF area-based Chinook abundance and transition probabilities, along with the median estimate of this fit (black line).

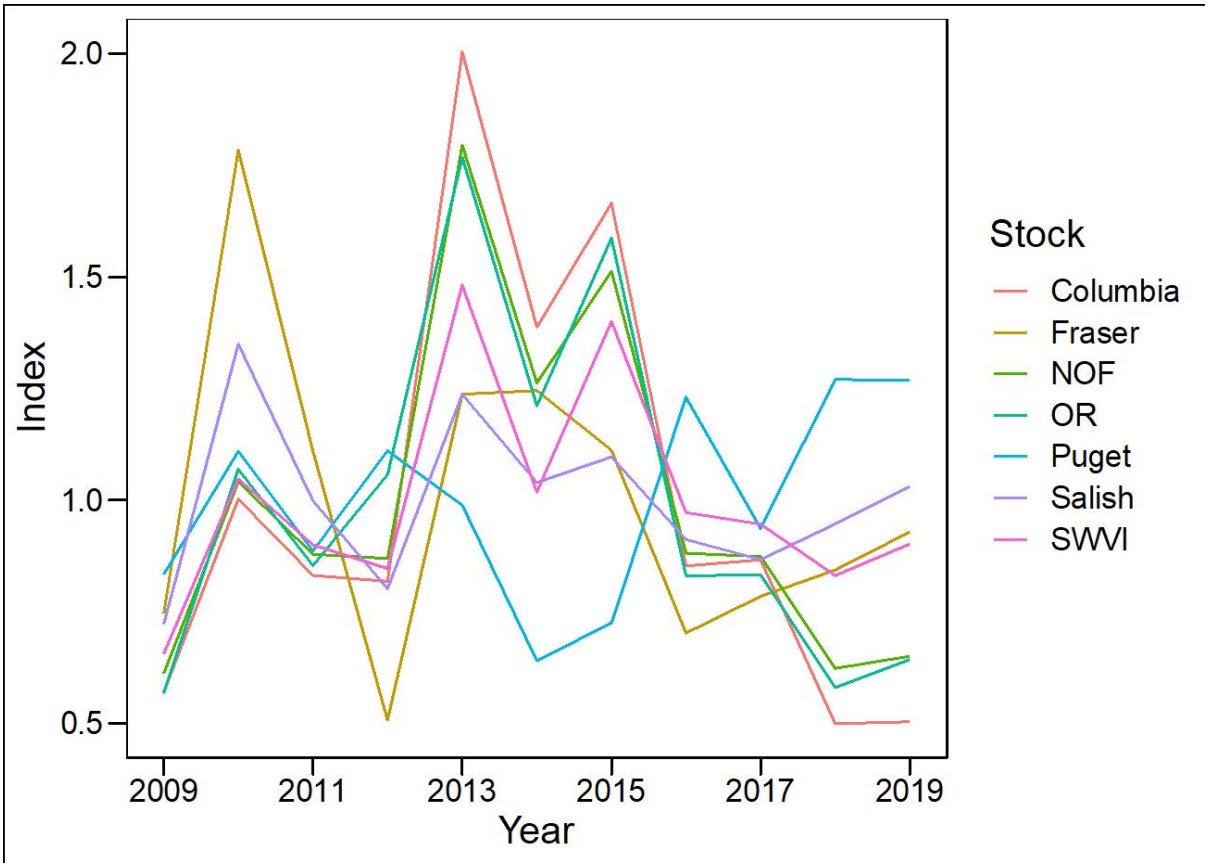

Figure S4. Chinook salmon abundances used as candidate covariates in the Southern Resident killer whale body condition transition models. The plotted abundance indices were generated by dividing the annual abundance for each stock by the mean abundance of that stock for years 2009-2019 in order to plot the salmon data on a common scale. The Columbia River, Fraser River, and Puget Sound are stock-specific abundance indices, while North of Cape Falcon (NOF), Oregon coast (OR), Salish Sea, and Southwest Vancouver Island (SWVI) are area-based Chinook abundance indices, representing total abundance of Chinook salmon from any stock within a specific region. See Methods for more details.